Atmos. Chem. Phys. Discuss., 15, 10939–10969, 2015
www.atmos-chem-phys-discuss.net/15/10939/2015/
doi:10.5194/acpd-15-10939-2015

Atmospheric Chemistry and Physics Discussions
Open Access

What is the limit of stratospheric sulfur climate engineering?

U. Niemeier and C. Timmreck

Max Planck Institute for Meteorology, Bundesstr. 53, 20146 Hamburg, Germany

Received: 1 April 2015 – Accepted: 1 April 2015 – Published: 15 April 2015

Correspondence to: U. Niemeier (ulrike.niemeier@mpimet.mpg.de)

Published by Copernicus Publications on behalf of the European Geosciences Union.

Abstract

The injection of sulfur dioxide (SO_2) into the stratosphere to form an artificial stratospheric aerosol layer is considered as an option for solar radiation management. The related reduction in radiative forcing depends upon the amount injected of sulfur dioxide but aerosol model studies indicate a decrease in forcing efficiency with increasing injection magnitude. None of these studies, however, consider injection strengths greater than $10\,Tg(S)\,yr^{-1}$. This would be necessary to counteract the strong anthropogenic forcing expected if "business as usual" emission conditions continue throughout this century. To understand the effects of the injection of larger amounts of SO_2 we have calculated the effects of SO_2 injections up to $100\,Tg(S)\,yr^{-1}$. We estimate the reliability of our results through consideration of various injection strategies, and from comparison with results obtained from other models. Our calculations show that the efficiency of the aerosol layer, expressed as the relationship between sulfate aerosol forcing and injection strength, decays exponentially. This result implies that the solar radiation management strategy required to keep temperatures constant at that anticipated for 2020, whilst maintaining "business as usual" conditions, would require atmospheric injections of the order of $45\,Tg(S)\,yr^{-1}$ which amounts to 6 times that emitted from of the Mt. Pinatubo eruption each year.

1 Introduction

Climate engineering (CE) aims to counteract anthropogenic forcing due to green house gas (GHG) emissions by reducing the amount of incoming solar radiation through solar radiation management (SRM). To estimate the climate impact of SRM, model comparison studies have been performed (Kravitz et al., 2011) to simulate mirrors in space (e.g., Schmidt et al., 2012) or stratospheric injection of sulfur dioxide (e.g., Pitari et al., 2013). Such injections, first suggested by Budyko (1977) and later by Crutzen (2006), follow the example of volcanic eruptions that naturally emit large amounts of SO_2 above

ACPD
15, 10939–10969, 2015

U. Niemeier and C. Timmreck

the tropopause. Chemical and microphysical reactions in this region result in the formation of sulfate aerosols that reduce, through solar reflection, the available solar radiation at the earth's surface and absorb outgoing longwave radiation in the stratosphere.

Initial studies of artificial sulfate aerosols estimated their effect on climate by performing climate model simulations with prescribed particle size and relatively vague assumptions for aerosol particle evolution (Rasch et al., 2008; Robock et al., 2008; Tilmes et al., 2009). A more comprehensive study, albeit two-dimensional, using a sectional aerosol microphysical model showed that the particle size distribution of the sulfate aerosol cloud depended strongly on the magnitude of the injections (Heckendorn et al., 2009). This has been confirmed by later studies (Pierce et al., 2010; Niemeier et al., 2011; Hommel and Graf, 2011; English et al., 2012) although the results differ in detail. The simulated particle size distribution differs considerably between models as does the poleward transport of stratospheric aerosol particles. These differences have implications for the estimated radiative forcing and hence on impact of the stratospheric aerosols on the climate.

These previous studies were performed with SO_2 injections of 1 to 10 Tg(S) yr^{-1}. Earth System Model studies, which aim to counteract anthropogenic forcing towards 2020 forcing conditions within the Geoengineering Model Intercomparison Project (GeoMIP, Kravitz et al., 2011), estimated sulfur emission strengths within this range. For example Niemeier et al. (2013) previously used up to 6 Tg(S) yr^{-1} to counteract 1.5 $W\,m^{-2}$ forcing of GHG as prescribed in the RCP4.5 scenario, defined in the fifth phase of the Climate Model Intercomparison Protocol (CMIP5, Taylor et al., 2012), for the second half of this century. Counteracting the forcing of the stronger GHG scenario RCP8.5 will require higher SO_2 injection rates.

With increasing emission strength the forcing efficiency, the ratio of sulfate aerosol forcing to injection strength, decreases (Heckendorn et al., 2009). This decrease in forcing efficiency is non-linear and the injected SO_2 amount needed to reduce strong GHG forcings will be high. We try, therefore, to estimate a theoretical upper limit for

ACPD
15, 10939–10969, 2015

possible SO_2 emissions after which a further increase in injection rate causes only a negligible decrease in radiative forcing.

We have performed simulations with the middle atmosphere version of the General Circulation Model (GCM) ECHAM5 (Roeckner et al., 2006; Giorgetta et al., 2006) interactively coupled to a modified version of the aerosol microphysical model HAM (Stier et al., 2005). This three-dimensional modal aerosol model allows for dynamical feedback on particle distribution. Particle size is a crucial parameter for the effectiveness of stratospheric aerosols as it influences absorption and scattering properties as well as the sedimentation velocity. ECHAM5-HAM simulations of increasing injection rates of up to 100 Tg(S) yr^{-1} will be analyzed regarding the efficiency of the injections (Sect. 3.1) followed by a discussion about injection strategies such as modification of the injection area size and different protocols defining the aerosol module (Sect. 3.2). We compare our results in Sect. 3.3 to those obtained from other models (Heckendorn et al., 2009; Pierce et al., 2010; English et al., 2012) to provide a broader perspective. In Sect. 4 we consider the limitation of SO_2 injection performed by other means.

2 Description of the model and the performed simulations

2.1 Model setup

The simulations for this study were performed with the middle atmosphere version of the GCM ECHAM5 (Giorgetta et al., 2006) with a spectral truncation at wave-number 42 (T42) and 39 vertical layers up to 0.01 hPa. The GCM solves prognostic equations for vorticity, divergence, surface pressure and temperature. In the applied model version the quasi-biennial oscillation (QBO) in the tropical stratosphere is not resolved and the model remains in a permanent east phase. The model runs in climate mode with fixed sea surface temperature.

The aerosol microphysical model HAM (Stier et al., 2005) is interactively coupled to the GCM, as well as to the radiation scheme of ECHAM5. The sulfate aerosol in-

ACPD
15, 10939–10969, 2015

fluences dynamical processes via temperature changes caused by scattering of shortwave radiation and absorption of near-infrared and longwave radiation. HAM calculates the sulfate aerosol formation including nucleation, accumulation, condensation and coagulation, as well as its removal processes via sedimentation and deposition.

The microphysical core of HAM, M7 (Vignati et al., 2004), was modified to allow better representation of the stratospheric sulfate aerosol. Nucleation was adapted to high SO_2 concentrations so when the number of molecules in the critical cluster is small (< 4) the collision rate of two molecules is calculated and used instead of the nucleation rate (Vehkamäki et al., 2002). The time stepping scheme for the H_2SO_4 gas equation is solved as described in Kokkola et al. (2009), which increased the accuracy of the model compared to previous versions (Wan et al., 2013). Within this stratospheric HAM version we treat only the sulfate aerosol and apart from the injected SO_2, only natural sulfur emissions are taken into account in the simulations. Further details are described by Niemeier et al. (2009).

The original modal setup of M7, i.e., with seven modes, represents tropospheric conditions and is not representative for the stratospheric sulfate aerosol. In accordance with box-model studies (Kokkola et al., 2009) we applied a special setup of the modes to describe stratospheric sulfate aerosols: one for simulations of volcanic eruptions (Volc) and one for SRM (Geo). Both are used in this study. The volcanic setup (Volc) contains no coarse mode and a smaller accumulation mode (standard deviation $\sigma = 1.2$). Model results using this setup show for e.g. particle size and radiation at top of the atmosphere (TOA) a good overall agreement with measured data taken after the Mt. Pinatubo eruption (Niemeier et al., 2009; Toohey et al., 2011). We see a slight overestimation of the poleward transport in the aerosol optical depth (AOD) compared to satellite measurements (Sato et al., 1993), and, consequently, calculated aerosol concentrations in the tropics were six months after the eruption lower than observed. The simulated tracer transport into the Southern Hemisphere after the Mt. Pinatubo eruption in June 1991 and the related AOD compare well with satellite measurements (Sato et al., 1993).

ACPD
15, 10939–10969, 2015

For simulations of SRM with sulfate aerosols the modal setup of M7 was further optimized to take into account the smaller sulfur flux (continuous emission) compared to those required for volcanic eruptions. Based on previous model comparisons (Kokkola et al., 2009) the SRM distribution includes a smaller standard deviation of the coarse mode ($\sigma = 1.2$ instead of 2) and the normal standard deviation of $\sigma = 1.59$ for the accumulation mode. As a result the simulated particle number distributions compares better to those described by a sectional aerosol model (Heckendorn et al., 2009). This SRM setup was used to calculate the amount of SO_2 emissions necessary to counterbalance anthropogenic forcing in the GeoMIP G3 experiment (Niemeier et al., 2013). The data from this model will be used as input data for a new GeoMIP intercomparison study (Tilmes et al., 2015).

The vertical resolution of ECHAM5 used for this study does not resolve the QBO. Previous studies show that the heated sulfate aerosol layer slows down the oscillation of the QBO and show an impact on the meridional tracer transport and the spatial and vertical distribution of the stratospheric aerosol, e.g. Plumb and Bell (1982); Punge et al. (2009); Aquila et al. (2014); Hommel et al. (2014). Based on these studies, we assume that the simulation of the QBO within our model would cause slight changes in the absolute values presented here but will not affect the validity of the main conclusions.

2.2 Setup of simulations

To study the dependence of the particle size distribution on the amount of injected SO_2 a series of numerical experiments were performed to simulate several years with continuous emissions between 1 and 100 Tg(S) yr^{-1}. SO_2 was injected at a height of 60 hPa (about 19 km) into one grid-box of a size of $2.8^\circ \times 2.8^\circ$ centered at the Equator at 121° E. In addition to the geoengineering setup, we used the volcanic setup for 100 Tg(S) yr^{-1} injection strength. All of the results presented here are averaged over at least three years of a steady global sulfur burden.

To estimate the uncertainty of the simulations, we varied the size of the injection area. For emissions of 10 Tg(S) yr^{-1} we increased the area of injections meridionally to 5° N and 5° S, and to 30° N and 30° S, as well as zonally to a one grid box wide circle along the Equator (Table 1). We do not alter the zonal position of the injection box because a case study by Toohey et al. (2011) revealed on average no significant longitudinal impact on tracer transport for a large tropical volcanic eruption. We also kept the injection height constant. The impact of the injection height was studied previously by Niemeier et al. (2011) indicating that increasing the injection height from 60 to 30 hPa also increases the efficiency due to a longer sedimentation path. Consequently increasing the injection height requires less injected SO_2 to obtain an equivalent reduction in radiative forcing.

Within this paper we concentrate on continuous injections with a continuous flux of tiny particles from the oxidation process of SO_2. Pulsed injections, studied previously by Heckendorn et al. (2009) and Niemeier et al. (2011), gave also an increased efficiency (see Sect. 3.2).

3 Results

In this study we aim to determine the efficiency of stratospheric SO_2 injections and their dependency on emission strength. The results are subject to several uncertainties, e.g. the modal setup and influence of injection area. We estimate their importance and impact on the presented results within this section. The efficiency of SO_2 injections is the ratio of top of the atmosphere (TOA) forcing to injection strength.

3.1 Impact of increasing injection rate

Figure 1 (left) shows the simulated global radiative fluxes at the top of the atmosphere (TOA) for different SO_2 injection rates. These data are derived from a double radiation call and describe the instantaneous aerosol forcing only. The orange curve shows the

Discussion Paper | Discussion Paper | Discussion Paper | Discussion Paper |

ACPD

15, 10939–10969, 2015

Limit of stratospheric sulfur climate engineering?

U. Niemeier and C. Timmreck

data for the TOA forcing (R_{TOA}), net shortwave (SW) plus net longwave (LW) radiation, for the different injection strengths. The simulations show a reduction of TOA forcing by −0.5, −2, −6, −8.5 W m^{-2} for emissions of 2, 10, 50, 100 Tg(S) yr^{-1}, respectively. The red curve in Fig. 1 (left) is a fit of the R_{TOA} as function of injection strength x (in Tg(S) yr^{-1}):

$$R_{TOA} = -65\,\mathrm{Wm}^{-2} \cdot e^{-\left(\frac{2246\,\mathrm{Tg(S)\,yr}^{-1}}{x}\right)^{0.23}}. \quad (1)$$

This fit to the simulated TOA imbalance extends the simulated R_{TOA} for even higher injection rates. Upon doubling the injection rate from 100 to 200 Tg(S) yr^{-1} the fitted exponential function yields a increase in the negativ forcing from −8.5 to roughly −12 W m^{-2}. Doubling of the injection strength, therefore, results in increase of only 40 % in the forcing.

A more detailed illustration of the radiative forcing efficiency at TOA is given in Fig. 1 (right), where the R_{TOA} is split in a SW and LW part. This figure clearly depicts that the decreasing radiative forcing efficiency results from the SW part. An injection of 5 Tg(S) yr^{-1} yields an efficiency of −0.23 W m^{-2} (Tg(S) yr^{-1})$^{-1}$ while an injection of 50 Tg(S) yr^{-1} yields an efficiency of −0.12 W m^{-2} (Tg(S) yr^{-1})$^{-1}$: a tenfold increase in injection results in 50 % reduction in the efficiency. This result can be explained by the plot in Fig. 2. For small injection rates (≤ 10 Tg(S) yr^{-1}) Fig. 2 shows that the number distribution is greater in accumulation mode than in coarse mode. As injection rates increase particle number and radii also increase in coarse mode. With increasing particle size scattering becomes less effective. The parallel curves of SW and R_{TOA} efficiency in Fig. 1 (right) indicate that the changes in scattering are mostly responsible for the decrease of R_{TOA} efficiency. In contrast, efficiency of LW radiation at TOA is almost constant and positive 0.1 W m^{-2} (Tg(S) yr^{-1})$^{-1}$. So the TOA LW flux anomalies contribute to the GHG effect instead of counterbalancing it.

Summarizing, the decrease in efficiency with increased injection strength follows exponential decay and is the consequence of the increased particle size that occurs

ACPD
15, 10939–10969, 2015

with increased injection strength. Larger particle radii result in decreased scattering of SW radiation and a shorter lifetime of the sulfate aerosol (Niemeier et al., 2011). LW absorption by the sulfate aerosol scales linearly per injected mass.

3.2 Range of results within one model

In this section we investigate the robustness of the values given in Fig. 1. The general performance of the global aerosol model has already been discussed in Sect. 2. Here, we test the robustness of our results by varying the injection area and by changing the internal M7 mode setup.

3.2.1 Impact of the size of the injection area – zonal extension

To further investigate the impact of the SO_2 injection flux per area the emission area in longitudinal or meridional directions for an injection rate of 10 Tg(S) yr^{-1} was increased. Table 2 gives the resulting global values of sulfur burden, AOD, top of the atmosphere forcing R_{TOA} and net SW radiation at TOA. The burden decreases with increasing injection area, as does AOD and R_{TOA}. R_{TOA} decreases by 12 % when SO_2 is injected zonally along the Equator instead of into a single grid box. The reason can be found in aerosol microphysical as well as in dynamical differences (see below).

The temporal microphysical evolution of the stratospheric sulfate aerosol is a competing process between nucleation, coagulation and condensation. The amount of nucleation or coagulation depends on the SO_2 flux into the stratosphere, as well as on the amount of existing particle (Heckendorn et al., 2009). An important difference between a case study of an explosive volcanic eruption and of a sulfur SRM application, as considered here, is the continuous sulfur emission flux. Freshly injected SO_2 is always available which has the following consequences for the microphysical processes of aerosol development:

1. Nucleation forms continuously small particles within the injection area.

ACPD
15, 10939–10969, 2015

2. H_2SO_4 is always available within the injection area to condense on these particles, the first growth step within the nucleation and Aitken modes.

3. Due to advection are larger particles in accumulation and coarse mode globally dispersed.

4. The coagulation coefficient depends on the ratio of radii between fine and coarse particles (Seinfeld and Pandis, 1998). The larger the ratio, the larger is the coagulation coefficient. This is most effective between fine ($r < 0.01$ µm) and coarse particles ($r > 1$ µm). As a consequence of the continuous emission flux under sulfur SRM are large and fine particle sizes always available. Hence coagulation has a stronger impact on particle size than condensation (Heckendorn et al., 2009) and is mostly responsible for the growth of coarse sized particles.

Figure 3 shows the distribution of SO_2 burden (top) and coarse mode sulfate particle burden (bottom) along the Equator for simulations Geo10 and Geo10-lon. For Geo10 the SO_2 burden is high within the injection area and SO_2 is advected to the West with burden values declining steeply. In Geo10-lon the constant emissions along the Equator result in an equal burden of about 10 mg m^{-3} of SO_2. This is almost one order of magnitude smaller than the maximum in Geo10 and an order of magnitude larger than the minimum in Geo10 around AREA-145. H_2SO_4 and nucleation mode particles behave similarly to SO_2 and occur mostly in the injection area as conversion processes occur quickly. In contrast to the distribution of precursor gases and the particle in the nucleation mode, the distribution of the coarse mode particle along the Equator in both simulations is almost equal (Fig. 3, bottom). This indicates that the lifetime of the coarse particles is longer than the zonal mixing time due to advection and diffusion and that transport plays an important role for the larger particles. The distribution of nucleation and Aitken mode particles is determined by microphysical processes only, while accumulation and coarse mode particle distributions depend on microphysical processes such as coagulation and transport.

Figure 4 shows on the left the aerosol number size distribution of Geo10 as an average over AREA-115 and AREA-145, and on the right the zonal average of Geo10 and Geo10-lon at the Equator. Compared to AREA-145 the number size distribution of AREA-115 shows high particle numbers in all modes, indicating that the processes of nucleation, condensation and coagulation are all in operation, especially new particle formation. In AREA-145 SO_2 concentration is low, consequently, the nucleation particle number and radius are both small. Additionally, low Aitken and accumulation mode numbers indicate small amounts of nucleation and condensation. This shows that the process of particle growth occurs mostly in, and downwind of, the injection area. In Geo10-lon injections occure along the Equator. The size number distribution of the zonal average, here representive for the injection area, is very similar to the one of AREA-115. For Geo10-lon both fine and large particles are available at all latitudes (Fig. 3) and the ratio of fine to large radii is large everywhere. Coagulation is, therefore, the dominant process everywhere and particles are able to grow in size. This decreases SW scattering and hence the forcing efficiency, by −12 % in R_{TOA} (Sect. 3.1).

Earlier studies (Heckendorn et al., 2009; Niemeier et al., 2011) suggest a similar effect when prolonging the time period of stratospheric injections. Changing the injection period from pulse to continuous decreases the injection flux but results over time in a more even distribution of particle and an overall quite regular availability of small particle. This results also in a decrease in efficiency.

3.2.2 Impact of the size of the injection area – meridional extension

The effect of increasing the size of the injection area in meridional direction was considered in simulation Geo10-5 and Geo10-30 (Table 1). For Geo10-5 the injection area is four times larger than for Geo10, for Geo10-30 20 times larger. The number size distribution in Fig. 5 (left) shows smaller values for the Aitken and accumulation modes for Geo10-30. This indicates a slight increase of coagulation in Geo10-30, resulting in a slight increase of the final particle size of the coarse mode.

ACPD
15, 10939–10969, 2015

The zonally averaged AOD (Fig. 5, right) reveals clear differences in the meridional distribution of sulfate in Geo10-30 between 30° N to 30° S compared to Geo10 and Geo10-5. The equal distribution of the injection over more latitudes reduces tropical AOD. The meridional cross sections of the zonal and annual mean of the SO_2 and sulfate concentrations (Fig. 6) show clear differences in the vertical distribution of SO_2 between Geo10 and Geo10-30. The temperature within the sulfate cloud is higher and the vertical velocity is about 10 % larger in Geo10 than in Geo10-30. The consequence is an increased vertical transport of the aerosols in the tropical stratosphere. The difference in the SO_2 and aerosol distribution is further related to stratospheric dynamics. At the boundary of the tropical region a subtropical transport barrier hinders meridional mixing (Brasseur and Solomon, 2005). ECHAM5-HAM results indicate that this transport barrier in a simulation without quasi-biennial oscillation is strongest around the latitude of 10° in the summer hemisphere (Punge et al., 2009). In Geo10-30 parts of the SO_2 emissions are outside of this barrier, thus meridional transport of SO_2 is greater (Fig. 6).

In summary, decreased efficiency is observed when the injection area is increased longitudinally. The zonally larger injectiona area causes a more even spread of precursor gases and fine particle. Coagulation is increased and this results in of the formation of larger particle radii and decreased SW scattering. The tropical transport barrier is an important factor when increasing the meridional injection area. Injecting outside of this barrier increases meridional transport and decreases the lifetime of the sulfate aerosol.

3.2.3 Impact of modal setup of HAM

HAM is a modal aerosol model, in which the aerosol size distribution is simplified by the use of four log-normal distributions, therefore, we have considered the uncertainty range related to the modal setup of our model. Kokkola et al. (2009) used a box model study of complex aerosol bin models to compare different modal setups of M7, the microphysical core of HAM. The results of the bin models showed that upon increasing the initial SO_2 concentration from 10^{-8} to 10^{-6} kg kg^{-1} the number distribution for radii $r > 0.1\,\mu m$ becomes mono-modal with a narrower mode width compared to standard M7. Consequently the simulation of a volcanic eruption with very high initial SO_2 concentrations required the development of parameters particular for this situation (Sect. 2). In Geo100, with a continuous injection rate of $100\,Tg(S)\,yr^{-1}$, the mean SO_2 concentration in AREA-115 is $3.5 \times 10^{-6}\,kg\,kg^{-1}$ which is within the range of large volcanic eruptions.

To estimate the resultant uncertainty, a simulation with the mono-modal volcanic setup for an injection rate of $100\,Tg(S)\,yr^{-1}$ (Volc100) was performed. Although the number size distribution between both modal set up differs, the difference in global AOD is only about 10 % and even less for R_{TOA} and the sulfur burden (Table 2). So although the efficiency of injections of approximately $100\,Tg(S)\,yr^{-1}$ may be slightly underestimated with the chosen set up, the TOA imbalance stays within the uncertainty range given for the different Geo10 experiments.

3.3 Comparison to other studies

Comparison of the ECHAM5-HAM results to those from other models is limited by the fact that a range of slightly different SRM experiments has been performed. The experiments differ in size and height of injection area and the studies determine different parameters. Comparison is, therefore, difficult and we limit ours to sulfur burden and AOD. We have compared our 3-D interactive GEO1-10 simulations with the results of two other model studies:

1. Pierce et al. (2010) (P10 thereafter) and (Heckendorn et al., 2009) (denoted H09 hereafter) used AER-2D (Weisenstein et al., 2007), a two dimensional sectional model. The aerosol is coupled to a radiation scheme.

2. English et al. (2012) (denoted E12 hereafter) used WACCM/CARMA which incorporates a three dimensional sectional aerosol model without coupling to a radiation scheme and is missing the dynamical impact of aerosol-induced heating in the stratosphere.

ACPD
15, 10939–10969, 2015

The different treatments of the aerosol (2-D vs. 3-D, sectional vs. modal) and the additional radiation scheme impact upon tracer transport. Together these experiments encompass the range of the uncertainties in the modeling of the relationship between SO_2 injection and TOA forcing.

Figure 7 (left) shows the global sulfate aerosol burden for the ECHAM5-HAM simulation (Geo1 to Geo10), as well as results of SRM studies by P10 and E12. Both studies include data for two injection areas: between 5° N to 5° S (narrow) and 30° N to 30° S (broad). The global burden values of ECHAM5-HAM Geo1 to Geo10 are quite similar to results of P10 and E12 (narrow), with a slightly greater slope in ECHAM5-HAM. The broad injection cases in P10 and E12 give roughly 30 and 60 % higher burden values than the narrow cases for injection strength of 10 Tg(S) yr^{-1}. That is, P10 and E12 efficiency is increased when the injection area spans more latitudes. These findings are different to those obtained from the Geo10 and Geo10-30 simulations, with 5 % decreases in the burden (Table 2). Why are the results between the models quite different?

In Sect. 3.2.2 we mentioned the importance of the tropical transport barrier on the tracer transport. From the presented results in H09, P10 and E12 we assume a strong barrier in both models. To show the differences between the results obtained in a model with strong or weak transport barrier we draw a simplified diagram of the zonally averaged AOD obtained for a narrow and a broad injection area (Fig. 7, right) after ECHAM5-HAM results and after estimated and simplified values from Fig. 9 in E12. The narrow cases show a distinct peak in the tropics, suggesting a meridional transport barrier in the tropical stratosphere, stronger in “NARROW” than that found in Geo10. The broad cases show an more even distribution of sulfate aerosol over all latitudes and for “BROAD” higher AOD at mid latitudes and polar regions than for “NARROW”. This shift of high ADO values from the tropics to mid latitudes indicates an increased meridional transport in “BROAD”. We assume that this, along with the consequent changes in aerosol evolution, is the main reason for the increase in sulfur burden with meridionally enlarged emission areas in E12 and P10. We see in ECHAM5-HAM an overall stronger

ACPD
15, 10939–10969, 2015

meridional transport than is the case in E12, along with a more permeable transport barrier. The difference between the burden resulting from narrow and broad injection areas in ECHAM5 is, therefore, smaller than in P10 and E12. It is also quite likely that the residence time of the particle in the extra tropics is shorter in ECHAM5-HAM.

It is important, therefore, to consider whether or not SO_2 is injected inside or outside the tropical transport barrier and how the permeability and the width of the barrier influence the meridional transport in the model. Heating of the sulfate aerosol is not incorporated into E12 and it is difficult to estimate its effect on results, however, meridional transport also depends on the vertical height of the aerosol. Niemeier et al. (2011) show less vertical transport in the tropics when switching of the coupling of aerosols to radiative processes.

4 What is the limit of sulfur injections?

The performed simulations have not given a final answer on the limit of SO_2 injections. The fitted curve in Fig. 1 describes an exponential decay and converges to $-65\,\mathrm{W\,m^{-2}}$, which is a high and uncertain theoretical limit, only achievable with infinitely high injections which is technically impossible. Can we, therefore, obtain a limit by other means? To do this we compare the injection rates to known measures such as flight emissions or injection efficiency given per achieved reduction of TOA forcing in $\mathrm{W\,m^{-2}}$. The injection efficiency gives the amount of sulfur per $\mathrm{W\,m^{-2}}$ which is needed to get a certain TOA forcing. These data show that to obtain a reduction of $-1\,\mathrm{W\,m^{-2}}$ an injection of $4.5\,\mathrm{Tg(S)\,yr^{-1}}$ per $\mathrm{W\,m^{-2}}$ is necessary, while $-7\,\mathrm{W\,m^{-2}}$ TOA forcing requires an injection of almost 10 Tg(S) per $\mathrm{W\,m^{-2}}$, so in total almost $70\,\mathrm{Tg(S)\,yr^{-1}}$. Mostly responsible for this decrease is the increase of particle radius which causes decreasing SW scattering and increased particle sedimentation (Sect. 3.1).

Robock et al. (2009) states that a US American F-15C Eagle can transport 8 t of sulfur gas at a height of 20 km. A reduction of RCP8.5 GHG forcing to RCP4.5 level at the end of the century, would require an TOA forcing reducion of $-4\,\mathrm{W\,m^{-2}}$ and an in-

ACPD
15, 10939–10969, 2015

jection of 26 Tg(S) yr^{-1}. This corresponds to around 3 millions flights per year, or about 6 Million flights if SO_2 would be transported, which is about half of the anthropogenic sulfur emissions in 2010 (Klimont et al., 2013). Compared to volcanic dimensions, this requires 3 to 4 Mt. Pinatubo eruptions per year, (7–8 Tg(S)), which was the strongest eruption in the last century.

Reducing TOA forcing to counteract RCP8.5 anthropogenic TOA forcing towards the end of the century to a level anticipated for 2020 would require a negative forcing of about 5.5 $W m^{-2}$ or an injection of 45 Tg(S) yr^{-1}. This would cause surface solar radiation to be reduced by 7 to 8 $W m^{-2}$, an overall 4 % decline (Liepert, 2002). 10 to 12 million flights would be necessary to transport this amount of SO_2 into the stratosphere. These estimates do not take into account the questions of sulfur production for the SRM injection or aeronautical logistics, both of which are substantial. The estimated numbers are certainly based on the ECHAM-HAM calculations including all model uncertainties discussed above. We have not considered indirect effects which may occur under high injection conditions. Changes of the QBO may alter tracer transport, which feeds back into aerosol microphysics. Additional nuclei for cloud condensation may get via sedimentation of sulfate aerosols into the upper troposphere and the resultant brighter clouds would reflect more sun light, a positive feedback. Besides the above described technical limitations, negative side-effects of sulfur SRM on society and environment might set a necessary limit, e.g. impact on ozone, sky brightness, changes in precipitation. The discussion of this is beyond the scope of the paper.

5 Conclusions

We have considered whether or not SO_2 injections into the stratosphere can theoretically counteract future anthropogenic CO_2 forcings as described in the RCP8.5 scenario. We investigated the efficiency of sulfur SRM, the ratio of TOA forcing to injection strength, with increasing SO_2 injections, as well as the influence of the size of the injection area. Our results show that with increasing injection strengths efficiency de-

ACPD
15, 10939–10969, 2015

creases. The curve of TOA forcing resulting from increasing injection strength of up to 100 Tg(S) yr^{-1} follows an exponential decay. The equation of the fit to this curve converges to −65 W m^{-2}. Hence, within the range of simulated injection strength this limit is far, even if we extrapolate the curve further to 200 Tg(S) yr^{-1}.

This study contribute to the discussion on the impact of changes of the injection flux on the efficiency, which shows a particular behaviour when changing the injection flux. Increasing the total injected amount, e.g. from 10 to 50 Tg(S) yr^{-1} increases the injection flux and the absolute forcing values, but reduces the forcing to injection ratio, thus decreases the efficiency. Increasing the injection flux per area by injecting into a smaller area, e.g. into a box instead of along the Equator, or per time by shortening the injection time, e.g. from continuous to pulsed injections, increases the absolute forcing but also the forcing efficiency. In both cases the nucleated particles are less even distributed. The consequence are changes in aerosol microphysical processes caused by the reduced availability of small particles outside of the injection area and period. Consequently the resulting particle size is smaller and scattering of SW radiation is more effective.

Enlarging the injection area meridionally within the tropical transport barrier around 10° N and 10° S has only a marginal impact on efficiency. Enlarging the injection area further and inject outside of the tropical transport barrier increases the meridional transport of aerosols. The consequences for the TOA forcing of the aerosol are a decrease of efficiency by 10 % in ECHAM5-HAM. Comparing this result to previous studies on the efficiency of injection strategies reveals large differences. While we found a decrease in efficiency when increasing the injection area meridionally English et al. (2012) and Pierce et al. (2010) obtain the opposite. Strength and location of the subtropical transport barrier as well as the poleward transport to high latitudes strongly influence the simulated latitudinal aerosol distribution and contribute therefore to the diverse response.

The answer to a limit of SO_2 injections provided here could therefore be quite different in details with other models. We described briefly the impact of tracer transport,

ACPD
15, 10939–10969, 2015

U. Niemeier and C. Timmreck

aerosol microphysical schemes and stratospheric dynamics. A clear answer to explain the reasons for the opposing results may be gained by a coordinated comparison of data on the microphysical evolution and the transport of a volcanic cloud obtained from the different models. In turn these results can be compared directly to empirical data. Such an approach is planned within the SPARC initiative SSIRC (www.sparc-ssirc.org) and partly within upcoming GeoMIP studies.

Acknowledgements. We thank Peter Irvine, Sebastian Rast, Alan Robock and Kai Zhang for inspiring discussions, Stefan Kinne and Ian Bytheway for valuable comments at different stages of the paper and Rene Hommel, Jan Kazil, Harri Kokkola and Hanna Vehkamäki for their earlier help to modify HAM. This work is a contribution to the German DFG-funded Priority Program “Climate Engineering: Risks, Challenges, Opportunities?” (SPP 1689). U. Niemeier is supported by the SPP 1689 within the project CEIBRAL. C. Timmreck acknowledges founding from the BMBF project MIKLIP (FKZ:01LP1130A). The simulations were performed on the computer of the Deutsches Klima Rechenzentrum (DKRZ). Information on the used data are available under: http://www.mpimet.mpg.de/en/staff/ulrike-niemeier/geoengineering/data.html.

The article processing charges for this open-access publication
were covered by the Max Planck Society.

References

Aquila, V., Garfinkel, C. I., Newman, P., Oman, L. D., and Waugh, D. W.: Modifications of the quasi-biennial oscillation by a geoengineering perturbation of the stratospheric aerosol layer, Geophys. Res. Lett., 41, 1738–1744, doi:10.1002/2013GL058818, 2014. 10944

Brasseur, G. and Solomon, S.: Aeronomy of the Middle Atmosphere, Springer, Dordrecht, the Netherlands, 2005. 10950

Budyko, M. I.: Climatic Changes, American Geophysical Society, Washington, DC, doi:10.1029/SP010, 1977. 10940

Crutzen, P. J.: Albedo enhancement by stratospheric sulfur injections: a contribution to resolve a policy dilemma?, Climatic Change, 77, 211–219, 2006. 10940

English, J. M., Toon, O. B., and Mills, M. J.: Microphysical simulations of sulfur burdens from stratospheric sulfur geoengineering, Atmos. Chem. Phys., 12, 4775–4793, doi:10.5194/acp-12-4775-2012, 2012. 10941, 10942, 10951, 10955, 10969

Giorgetta, M. A., Manzini, E., Roeckner, E., Esch, M., and Bengtsson, L.: Climatology and forcing of the quasi–biennial oscillation in the MAECHAM5 model, J. Climate, 19, 3882–3901, 2006. 10942

Heckendorn, P., Weisenstein, D., Fueglistaler, S., Luo, B. P., Rozanov, E., Schraner, M., Thomason, L. W., and Peter, T.: The impact of geoengineering aerosols on stratospheric temperature and ozone, Environ. Res. Lett., 4, 045108, doi:10.1088/1748-9326/4/4/045108, 2009. 10941, 10942, 10944, 10945, 10947, 10948, 10949, 10951

Hommel, R. and Graf, H.: Modelling the size distribution of geoengineered stratospheric aerosols, Atmos. Sci. Lett., 12, 168–175, doi:10.1002/asl.285, 2011. 10941

Hommel, R., Timmreck, C., Giorgetta, M. A., and Graf, H. F.: Quasi-biennial oscillation of the tropical stratospheric aerosol layer, Atmos. Chem. Phys. Discuss., 14, 16243–16290, doi:10.5194/acpd-14-16243-2014, 2014. 10944

Klimont, Z., Smith, S., and Cofala, J.: The last decade of global anthropogenic sulfur dioxide: 2000-2011 emissions, Environ. Res. Lett., 8, 014003, doi:10.1088/1748-9326/8/1/014003, 2013. 10954

Kokkola, H., Hommel, R., Kazil, J., Niemeier, U., Partanen, A.-I., Feichter, J., and Timmreck, C.: Aerosol microphysics modules in the framework of the ECHAM5 climate model – intercomparison under stratospheric conditions, Geosci. Model Dev., 2, 97–112, doi:10.5194/gmd-2-97-2009, 2009. 10943, 10944, 10950

Kravitz, B., Robock, A., Boucher, O., Schmidt, H., Taylor, K. E., Stenchikov, G., and Schulz, M.: The Geoengineering Model Intercomparison Project (GeoMIP), Atmos. Sci. Lett., 12, 162–167, doi:10.1002/asl.316, 2011. 10940, 10941

Liepert, B. G.: Observed reductions of surface solar radiation at sites in the United States and worldwide from 1961 to 1990, Geophys. Res. Lett., 29, 61.1–61.4, doi:10.1029/2002GL014910, 2002. 10954

Niemeier, U., Timmreck, C., Graf, H.-F., Kinne, S., Rast, S., and Self, S.: Initial fate of fine ash and sulfur from large volcanic eruptions, Atmos. Chem. Phys., 9, 9043–9057, doi:10.5194/acp-9-9043-2009, 2009. 10943

Discussion Paper | Discussion Paper | Discussion Paper | Discussion Paper |

ACPD

15, 10939–10969, 2015

Limit of stratospheric sulfur climate engineering?

U. Niemeier and C. Timmreck

Niemeier, U., Schmidt, H., and Timmreck, C.: The dependency of geoengineered sulfate aerosol on the emission strategy, Atmos. Sci. Lett., 12, 189–194, doi:10.1002/asl.304, 2011. 10941, 10945, 10947, 10949, 10953

Niemeier, U., Schmidt, H., Alterskjær, K., and Kristjánsson, J. E.: Solar irradiance reduction via climate engineering – Impact of different techniques on the energy balance and the hydrological cycle, J. Geophys. Res., 118, 11905–11917, doi:10.1002/2013JD020445, 2013. 10941, 10944

Pierce, J. R., Weisenstein, D. K., Heckendorn, P., Peter, T., and Keith, D. W.: Efficient formation of stratospheric aerosol for climate engineering by emission of condensible vapor from aircraft, Geophys. Res. Lett., 37, L18805, doi:10.1029/2010GL043975, 2010. 10941, 10942, 10951, 10955, 10964, 10969

Pitari, G., Aquila, V., Kravitz, B., Robock, A., Watanabe, S., Luca, N. D., Genova, G. D., Mancini, E., Tilmes, S., and Cionni, I.: Stratospheric ozone response to sulfate geoengineering: results from the Geoengineering Model Intercomparison Project (GeoMIP), J. Geophys. Res., 119, 2629–2653, doi:10.1002/2013JD020566, 2013. 10940

Plumb, R. A. and Bell, R. C.: A model of quasibiennial oscillation on an equatorial beta-plane, Q. J. Roy. Meteor. Soc., 108, 335–352, 1982. 10944

Punge, H. J., Konopka, P., Giorgetta, M. A., and Müller, R.: Effects of the quasi-biennial oscillation on low-latitude transport in the stratosphere derived from trajectory calculations, J. Geophys. Res., 114, D03102, doi:10.1029/2008JD010518, 2009. 10944, 10950

Rasch, P. J., Crutzen, P. J., and Coleman, D. B.: Exploring the geoengineering of climate using stratospheric sulfate aerosols: the role of particle size, Geophys. Res. Lett., 35, L02809, doi:10.1029/2007GL032179, 2008. 10941

Robock, A., Oman, L., and Stenchikov, G. L.: Regional climate responses to geoengineering with tropical and Arctic SO_2 injections, J. Geophys. Res., 113, D16101, doi:10.1029/2008JD010050, 2008. 10941

Robock, A., Marquardt, A., Kravitz, B., and Stenchikov, G.: Benefits, risks, and costs of stratospheric geoengineering, Geophys. Res. Lett., 36, L19703, doi:10.1029/2009GL039209, 2009. 10953

Roeckner, E., Brokopf, R., Esch, M., Giorgetta, M., Hagemann, S., Kornblueh, L., Manzini, E., Schlese, U., and Schulzweida, U.: Sensitivity of simulated climate to horizontal and vertical resolution in the ECHAM5 atmosphere model, J. Climate, 19, 3771–3791, 2006. 10942

ACPD
15, 10939–10969, 2015

Limit of stratospheric sulfur climate engineering?

U. Niemeier and C. Timmreck

Sato, M., Hansen, J. E., McCormick, M. P., and Pollack, J. B.: Stratospheric aerosol optical depths, J. Geophys. Res., 98, 22987, doi:10.1029/93JD02553, 1993. 10943

Schmidt, H., Alterskjær, K., Bou Karam, D., Boucher, O., Jones, A., Kristjánsson, J. E., Niemeier, U., Schulz, M., Aaheim, A., Benduhn, F., Lawrence, M., and Timmreck, C.: Solar irradiance reduction to counteract radiative forcing from a quadrupling of CO_2: climate responses simulated by four earth system models, Earth Syst. Dynam., 3, 63–78, doi:10.5194/esd-3-63-2012, 2012. 10940

Seinfeld, J. H. and Pandis, S. N.: Atmospheric Chemistry and Physics: From Air Pollution to Climate Change, Wiley-Interscience, New York, 1998. 10948

Stier, P., Feichter, J., Kinne, S., Kloster, S., Vignati, E., Wilson, J., Ganzeveld, L., Tegen, I., Werner, M., Balkanski, Y., Schulz, M., Boucher, O., Minikin, A., and Petzold, A.: The aerosol-climate model ECHAM5-HAM, Atmos. Chem. Phys., 5, 1125–1156, doi:10.5194/acp-5-1125-2005, 2005. 10942

Taylor, K. E., Stouffer, R. J., and Meehl, G. A.: An Overview of CMIP5 and the experiment design, B. Am. Meteorol. Soc., 93, 485–498, doi:10.1175/BAMS-D-11-00094.1, 2012. 10941

Tilmes, S., Garcia, R. R., Kinnison, D. E., Gettelman, A., and Rasch, P. J.: Impact of geo-engineered aerosols on the troposphere and stratosphere, J. Geophys. Res., 114, D12305, doi:10.1029/2008JD011420, 2009. 10941

Tilmes, S., Mills, M. J., Niemeier, U., Schmidt, H., Robock, A., Kravitz, B., Lamarque, J.-F., Pitari, G., and English, J. M.: A new Geoengineering Model Intercomparison Project (GeoMIP) experiment designed for climate and chemistry models, Geosci. Model Dev., 8, 43–49, doi:10.5194/gmd-8-43-2015, 2015. 10944

Toohey, M., Krüger, K., Niemeier, U., and Timmreck, C.: The influence of eruption season on the global aerosol evolution and radiative impact of tropical volcanic eruptions, Atmos. Chem. Phys., 11, 12351–12367, doi:10.5194/acp-11-12351-2011, 2011. 10943, 10945

Vehkamäki, H., Kulmala, M., Napari, I., Lehtinen, K. E. J., Timmreck, C., Noppel, M., and Laaksonen, A.: An improved parameterization for sulfuric acid water nucleation rates for tropospheric and stratospheric conditions, J. Geophys. Res., 107, 4622–4632, 2002. 10943

Vignati, E., Wilson, J., and Stier, P.: M7: An efficient size resolved aerosol microphysics module for large–scale aerosol transport models, J. Geophys. Res., 109, D22202, doi:10.1029/2003JD004485, 2004. 10943

Wan, H., Rasch, P. J., Zhang, K., Kazil, J., and Leung, L. R.: Numerical issues associated with compensating and competing processes in climate models: an example from ECHAM-HAM, Geosci. Model Dev., 6, 861–874, doi:10.5194/gmd-6-861-2013, 2013. 10943

Weisenstein, D. K., Penner, J. E., Herzog, M., and Liu, X.: Global 2-D intercomparison of sectional and modal aerosol modules, Atmos. Chem. Phys., 7, 2339–2355, doi:10.5194/acp-7-2339-2007, 2007. 10951

ACPD

15, 10939–10969, 2015

Limit of stratospheric sulfur climate engineering?

U. Niemeier and C. Timmreck

Table 1. Overview of the input parameters for the simulations performed with ECHAM5-HAM. The injection rate differs between the simulations, as well as the injection area and the mode configuration of the aerosol microphysics. Lonbox is one grid box at the Equator at 120.9 to 123.75° E

Simulation	Rate $Tg(S)\,yr^{-1}$	Area	Mode setup
Geo	1, 2, 3, 4, 5, 6, 8, 10, 20, 30, 40, 50, 70, 100	2.8° N to Equator lonbox	geoeng.
Geo10-5	10	5° N to 5° S lonbox	geoeng.
Geo10-30	10	30° N to 30° S lonbox	geoeng.
Geo10-lon	10	2.8° N to Equator all longitudes	geoeng.
Volc100	100	2.8° N to Equator lonbox	volc.

ACPD
15, 10939–10969, 2015

Table 2. Burden, AOD, R_{TOA} (net SW + LW), and net surface SW radiation for the different simulations. R_{diff} is the relative difference of R_{TOA} to Geo10 and Geo100.

Simulation Unit	Burden Tg(S)	AOD	R_{TOA} $W m^{-2}$	R_{diff} %	SW_{srf} $W m^{-2}$
Geo10	6.44	0.18	−2.03	–	−2.55
Geo10-5	6.36	0.17	−2.06	−1.5	−2.52
Geo10-30	6.16	0.15	−1.81	−11	−2.3
Geo10-lon	5.98	0.14	−1.79	−12	−2.3
Geo100	62.3	0.79	−8.46	–	−14.9
Volc100	61.8	0.89	−9.01	6	−15.43

ACPD
15, 10939–10969, 2015

Limit of stratospheric sulfur climate engineering?

U. Niemeier and C. Timmreck

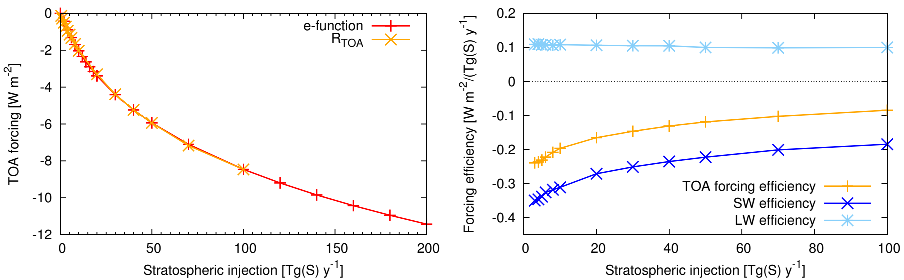

Figure 1. (Left) Top of the atmosphere (TOA) radiative fluxes (net shortwave plus net longwave, orange) and exponential fit of TOA forcing (red) (Eq. 1) for different injection rates. (Right) Forcing efficiency of TOA radiative forcing, forcing per injection [$Wm^{-2}\,(Tg(S)\,yr^{-1})^{-1}$], for R_{TOA} (orange), SW and LW radiation (blue).

ACPD
15, 10939–10969, 2015

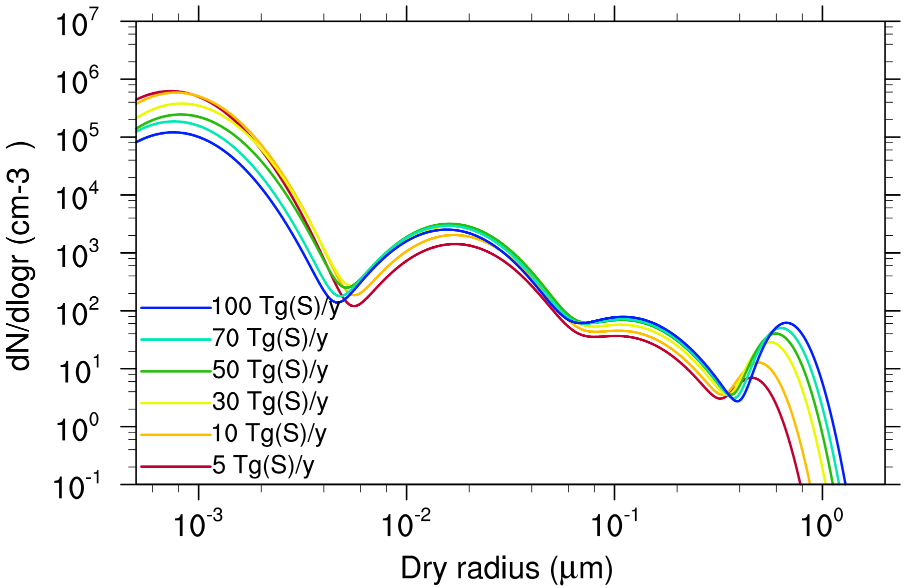

Figure 2. Zonally averaged aerosol number size distribution at 54 hPa height at the Equator for different injection rates. Given are values for nucleation mode (Radius (r) ≤ 5 nm), Aitken mode (5 nm ≤ r ≤ 50 nm), accumulation mode (0.05 µm ≤ r ≤ 0.2 µm) and coarse mode (r ≥ 0.2 µm). Radiative active are only particle in accumulation and coarse mode. Scattering of SW radiation is strongest in accumulation mode and gets less effective with increasing particle size (Pierce et al., 2010).

ACPD
15, 10939–10969, 2015

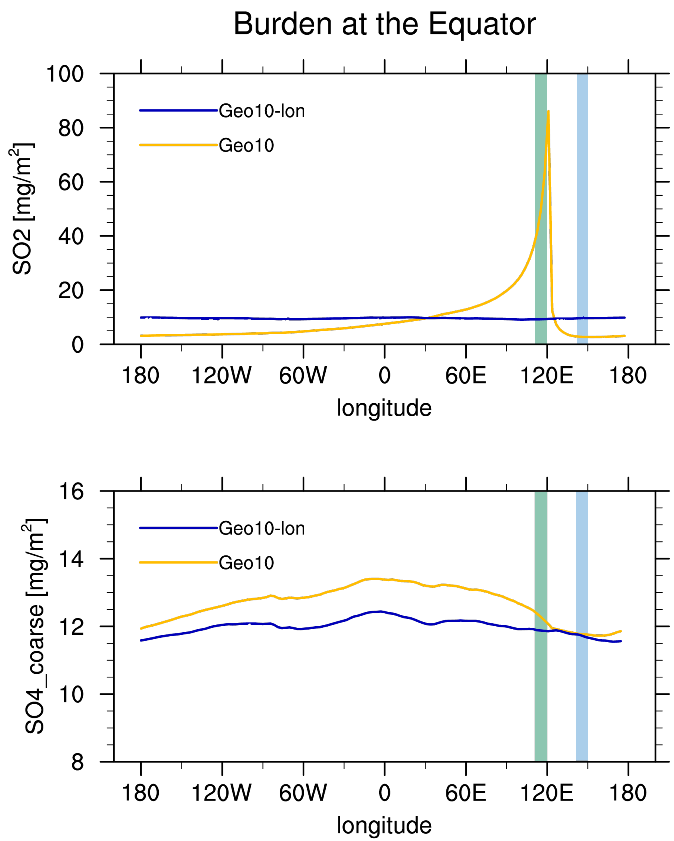

Figure 3. Burden of SO_2 and sulfate coarse mode particles in a one grid box wide area along the Equator for two different simulations. Within the two marked areas concentrations are averaged for Fig. 4: downwind of the injection area at 110 to 120° E (green area, named AREA-115 later) and upwind to the injection area at 140 to 150° E (blue area, AREA-145). Meridionally both areas are one model grid box wide, from the Equator to 2.8° N.

ACPD
15, 10939–10969, 2015

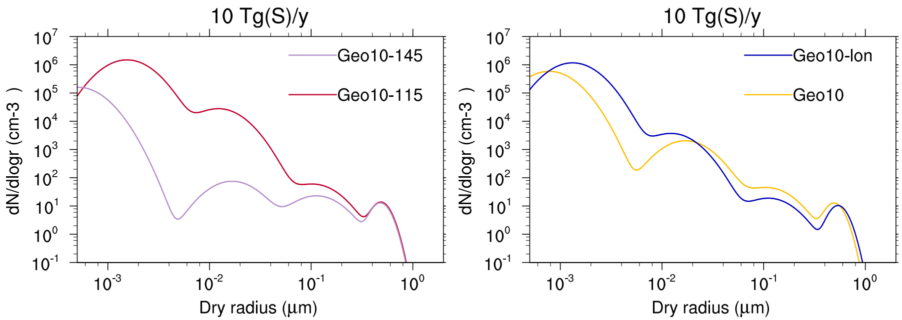

Figure 4. Aerosol number size distribution of particles in a height of 54 hPa at the Equator for injection rates of 10 Tg(S) yr^{-1}. (Left) Geo10 averaged over a 10° wide area upwind (AREA-145) and downwind (AREA-115) of the injection area (see also Fig. 3). (Right) Zonal average of Geo10 and Geo10-lon.

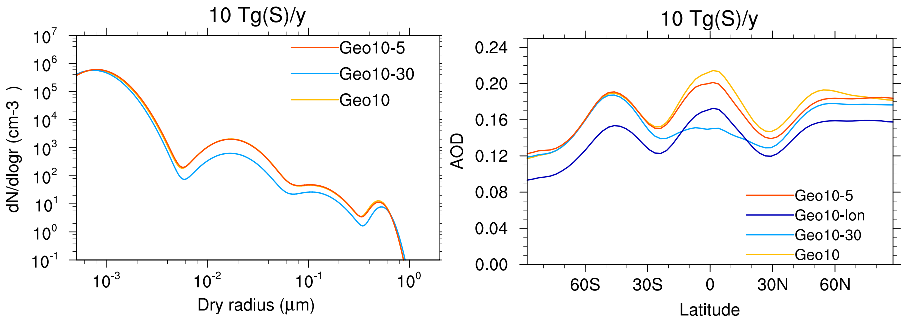

Figure 5. Zonally averaged data of aerosol number size distribution (left) and AOD (right) for experiments with different injection rates of 10 Tg(S) yr^{-1}. Each plot shows results of experiments with varying extend of the injection area in zonal (Geo10-lon) and meridional (Geo10-5, Geo10-30) direction.

ACPD
15, 10939–10969, 2015

U. Niemeier and C. Timmreck

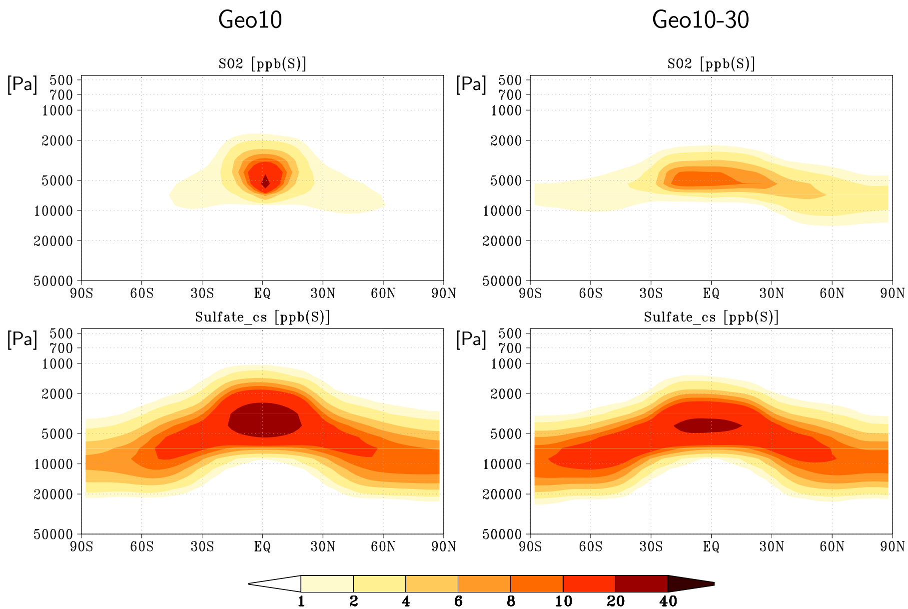

Figure 6. Zonally and annually averaged SO_2 (top) and sulfate coarse mode (bottom) concentration for Geo10 (left) and Geo10-30 (right) experiments with injection rates of 10 Tg(S) yr^{-1}.

ACPD
15, 10939–10969, 2015

Limit of stratospheric sulfur climate engineering?

U. Niemeier and C. Timmreck

Title Page
Abstract Introduction
Conclusions References
Tables Figures
◀◀ ▶▶
◀ ▶
Back Close
Full Screen / Esc
Printer-friendly Version
Interactive Discussion

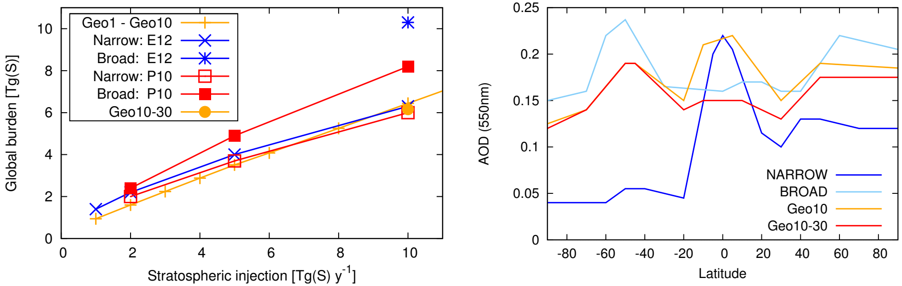

Figure 7. Left: global sulfate aerosol burden for ECHAM5-HAM simulations Geo1 to Geo10 and results from Pierce et al. (2010) and English et al. (2012) for two different emission areas. Narrow: 5° N to 5° S and Broad: 30° N to 30° S, both for longitudinal emissions. Right: simplified diagram of AOD for a narrow and a broad injection area case in two different models: Geo10 and Geo10-30 after ECHAM5-HAM results and NARROW and BROAD estimated from English et al. (2012).

ACPD
15, 10939–10969, 2015

Limit of stratospheric sulfur climate engineering?

U. Niemeier and C. Timmreck